Electronic Supplementary Material (ESI) for Physical Chemistry Chemical Physics.

Supplementary Information

Silver-Gold alloy nanoparticle as tunable substrates for systematic control of ion desorption efficiency and heat transfer in surface-assisted laser desorption/ionization

Samuel Kin-Man Lai, Yu-Hong Cheng, Ho-Wai Tang, and Kwan-Ming Ng*

Department of Chemistry, The University of Hong Kong, Pokfulam Road, Hong Kong SAR, People's Republic of China

*** To whom correspondence should be addressed:**

KM Ng, email: kwanmng@hku.hk

S1.A Analysis of Nanoparticles Prepared by Argon Ion Sputtering

The section area of a single NP was calculated based on: $(\text{particle radius})^2 \times \pi$. The average particle size of NPs was obtained from three TEM micrographs to obtain a representative evaluation of the particle size distribution. The results were summarized in **Table S1**.

The average number of NPs in a TEM micrograph was multiplied by the area ratio (9.12×10^8) between the area of a 3 mm-diameter MALDI sample well and the area of a TEM micrograph in order to estimate the total number of particles in a 3 mm-diameter MALDI sample well:

No. of NPs in a MALDI sample well = (No. of NPs in TEM micrograph) × (9.12×10^8)

Multiplying total number of NPs in a 3 mm-diameter MALDI sample well with the section area of a single NP gives the total coverage section area of NPs in a 3 mm-diameter MALDI sample well:

Total Coverage Section Area of NPs in a MALDI Sample Well = (No. of NPs in a MALDI sample well) × (section area of a single NP)

Table S1. Particle analysis results for AuNPs, Ag15Au85NPs, Ag55Au45NPs, AgNPs using ImageJ (version 1.45s, NIH, U.S.A.).

	Average Diameter (Mean ± SD nm) $[a]$	Average Number of NPs in a TEM micrograph covering an area of 88 × 88 nm^2 $[b]$	Average Coverage Section Area (nm^2) of NPs in a TEM micrograph covering an area of 88 × 88 nm^2 $[c] = (\frac{[a]}{2})^2 \times \pi \times [b]$
AuNPs	1.87 ± 0.32	384	1086
Ag15Au85NPs	1.67 ± 0.32	442	1006
Ag55Au45NPs	1.85 ± 0.34	308	854
AgNPs	2.39 ± 0.71	44	215

S1.B Calculation of Normalized BP Ion Intensity and UV-Visible Absorbance

The normalized total intensity of BP ion and UV-Visible Absorbance were calculated by dividing the measured UV-Visible absorbance or total ion intensity with the total coverage section area of NPs in a MALDI sample well, and expressed as arbitrary unit/mm^2 and count/mm^2

$$\text{Normalized Total Ion Intensity} = \frac{\text{Total Intensity of BP Ion detected from a MALDI Sample Well}}{\text{Total Coverage Section Area of NPs in a 3 mm MALDI Sample Well}}$$

$$\text{Normalized UV Absorbance} = \frac{\text{Measured Absorbance}}{\text{Total Coverage Section Area of NPs in a 3 mm MALDI Sample Well}}$$

S2. Elemental Composition Analysis of Ag-Au Alloy NPs by Energy-Dispersive X-ray Spectroscopy

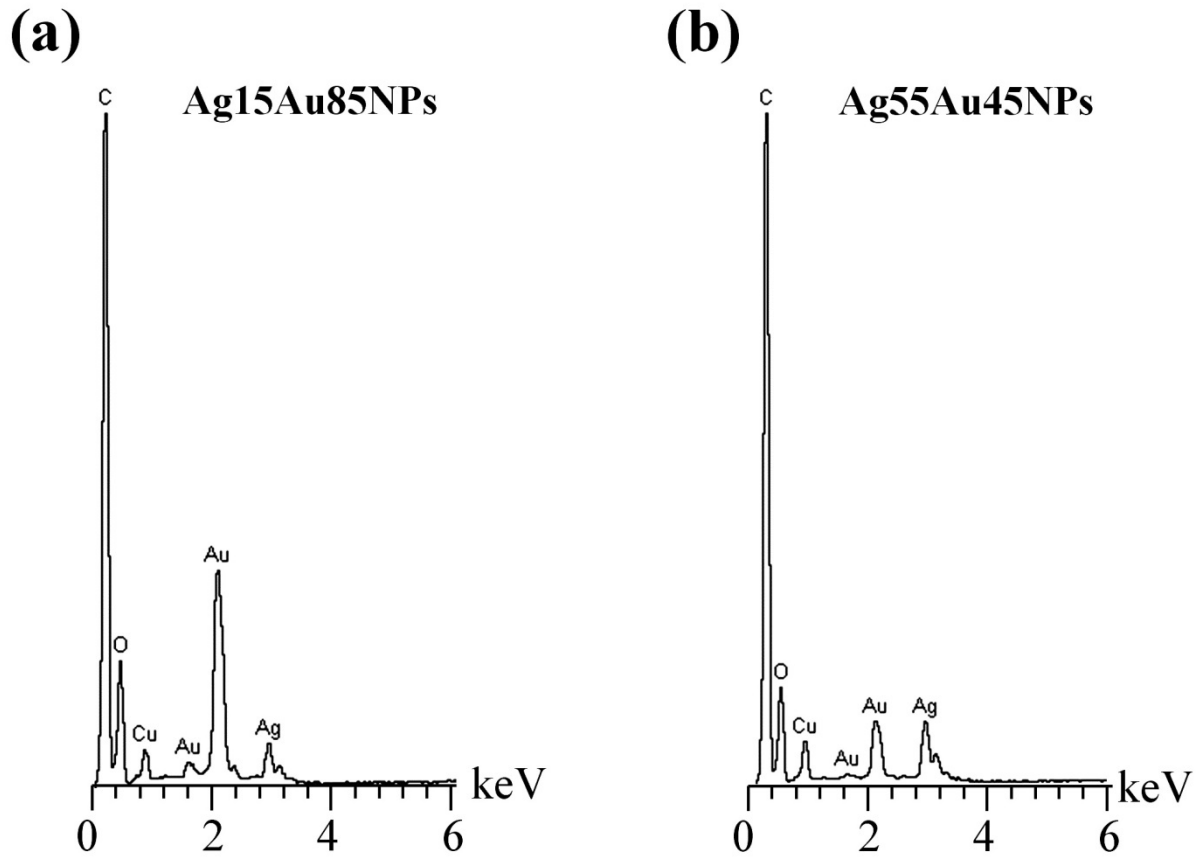

Figure S1. Energy-dispersive X-ray spectroscopy (EDS) spectrum of (a) Ag15Au85NPs and (b) Ag55Au45NPs prepared by argon ion sputtering using Ag20Au80 and Ag60Au40 targets respectively. [Remarks: Presence of C, O, and Cu were due to the copper grid and the supporting formvar film used in Transmission Electron Microscopy.]

S3. Comparison of Two Sets of MEAM Parameters for the Simulation

Second-nearest-neighbor modified embedded-atom potentials (MEAM-2nn) were employed for the simulation of dynamics of laser irradiated metal NPs. Here, we attempted to compare the accuracy of two sets of MEAM parameters in modelling laser irradiated AgNPs and AuNPs.

The first set of the parameters was developed by Lee, B.J *et al.*, [1] which was the same as the one used in our previous study on noble metal NPs. [2] **(Table S2)** Employing this set of parameters in the MEAM-2nn potential, the predicted melting point of AuNP (835 K) is consistent with the experimental scanning electron diffraction measurements (~825 K). [3] However, the predicted melting point of AgNP (795 K) was much higher than the experimental value (450 K). [4] Thus, the simulation was also repeated with another set of MEAM parameters **(Table S3)** built in the LAMMPS package [5-6], in order to have a better agreement with the experimental data.

Table S2. Parameters for the MEAM potential of Ag and Au from Lee, B. J's work. E_i^0 is the sublimation energy (eV), R_i^0 is the equilibrium nearest-neighbor distance (Å), α_i is the exponential decay factor for the universal energy function, A_i is the scaling factor for the embedding energy, $\beta_i^{(0)}$are the exponential decay factors for the atomic densities while $t_i^{(l)}$are the weighting factors for the atomic densities.

	E_i^0	R_i^0	α_i	A_i	$\beta_i^{(0)}$	$\beta_i^{(1)}$	$\beta_i^{(2)}$	$\beta_i^{(3)}$	$t_i^{(1)}$	$t_i^{(2)}$	$t_i^{(3)}$
Ag	2.85	2.88	6.01	0.94	4.73	2.20	6.00	2.20	3.40	3.00	1.50
Au	3.93	2.88	6.60	1.00	5.77	2.20	6.00	2.20	2.90	1.64	2.00

Table S3. Parameters for the MEAM potential of Ag and Au built in the LAMMPS package.

	E_i^0	R_i^0	α_i	A_i	$\beta_i^{(0)}$	$\beta_i^{(1)}$	$\beta_i^{(2)}$	$\beta_i^{(3)}$	$t_i^{(1)}$	$t_i^{(2)}$	$t_i^{(3)}$
Ag	2.85	2.88	5.89	1.06	4.46	2.20	6.00	2.20	5.54	2.45	1.29
Au	3.93	2.88	6.34	1.04	5.45	2.20	6.00	2.20	1.56	1.51	2.61

Employing the LAMMPS embedded MEAM parameters in MEAM-2nn potential, it was found that the predicted melting point for AuNP (835 K) was also highly consistent with previous experimental result (~825K). Furthermore, it predicted a melting point (560 K) that is much closer to the experimental value (450 K) for AgNPs. **(Table S4)** Due to the better accuracy, this set of parameters was used for the simulation of dynamics of both pure and alloys NPs.

Table S4. Comparison of melting points of 2.5 nm AgNP and AuNP computed employing two different set of MEAM parameters in MEAM-2nn potential.

	Melting Point (K)		
	MEAM Parameters Adopted from Lee, B.J's Work [1]	**MEAM Parameters Embedded in LAMMPS*[5-6]**	**Experimental Values**
AgNP	795	560	~ 450† [4]
AuNP	835	835	~ 825‡ [3]

***** MEAM Parameters Embedded in the LAMMPS package was decisively adopted in this study.

† Result of real time spectroscopic ellipsometry measurements

‡ Result of scanning electron diffraction measurements

S4. Calculation of Absorption Coefficients of Nanoparticles Using Mie Theory

From the definition, the absorption coefficients of metallic NPs are directly proportional to its absorption cross section. (**Eq. S4.1**) [7]

$$\alpha(\lambda) = N \times C_{abs}(\lambda) \qquad \textbf{Eq. S4. 1}$$

Where $\alpha(\lambda)$ (cm^{-1}) is the absorption coefficients at wavelength λ, N is the atomic number density (0.0015 nm^{-3}) of the NPs, and $C_{abs}(\lambda)$ (cm^2) is the absorption cross section at wavelength λ.

According to Mie theory, the absorption cross section, $C_{abs}(\lambda)$, of metallic NPs upon electromagnetic irradiation at a wavelength, λ, could be calculated from Mie coefficients, which is dependent on the size of the NP and relative refractive index between the NP and the surrounding medium. (**Eq. S4.2**) [7]

$$C_{abs}(\lambda) = \frac{2\pi}{k^2}\sum_{n=1}^{\infty}(2n+1)[Re(a_n + b_n) - (|a_n|^2 + |b_n|^2)] \qquad \textbf{Eq. S4. 2}$$

Where $k = \frac{2\pi n}{\lambda}$, a_n and b_n are Mie coefficients defined by the following expressions (**Eq. S4.3a** and **Eq. S4.3b**):

$$a_n = \frac{m\psi_n(mx)\psi_n{}'(x) - \psi_n(x)\psi_n{}'(mx)}{m\psi_n(mx)\xi_n{}'(x) - \xi_n(x)\psi_n{}'(mx)} \qquad \textbf{Eq. S4. 3a}$$

$$b_n = \frac{\psi_n(mx)\psi_n{}'(x) - m\psi_n(x)\psi_n{}'(mx)}{\psi_n(mx)\xi_n{}'(x) - m\xi_n(x)\psi_n{}'(mx)} \qquad \textbf{Eq. S4. 3b}$$

Where x is the size parameter dependent on the radius of the NP (R) (**Eq. S4.4a**) and, m is the relative refractive index between the NP, $n_{NP}(\lambda)$, and the surrounding medium, $n_{med}(\lambda)$ (1 for vacuum) (**Eq. S4.4b**).

$$x = kR = \frac{2\pi R}{\lambda} \qquad \textbf{Eq. S4. 4a}$$

$$m = \frac{n_{NP}(\lambda)}{n_{med}(\lambda)} \qquad \textbf{Eq. S4. 4b}$$

$\psi_n(x)$ (**Eq. S4.5a)** and $\xi_n(x)$ (**Eq. S4.5b)** are *Ricatti-Bessal* functions: [8]

$$\psi_n(x) = x j_n(x) \qquad \textbf{Eq. S4. 5a}$$

$$\xi_n(x) = x h_n^{(1)}(x) \qquad \textbf{Eq. S4. 5b}$$

The refractive index of NP (n_{NP}) used in calculation of Mie coefficients could be obtained from the representative dielectric functions of corresponding NPs. (**Eq. S4.6**)

$$n_{NP}(\lambda) = \sqrt{\varepsilon_{NP}(\lambda)} \qquad \textbf{Eq. S4. 6}$$

Where $\varepsilon_{NP}(\lambda)$ is the dielectric function of the NP at wavelength λ.

The dielectric functions of the Ag-Au alloys were calculated using a linear relationship on the volume fraction, as expressed in **Eq. S4.7**. [9-10]

$$\varepsilon_{alloy}(\rho_{Ag}, \lambda) = \rho_{Ag}\varepsilon_{Ag}(\lambda) + (1 - \rho_{Ag})\varepsilon_{Au}(\lambda) \qquad \textbf{Eq. S4. 7}$$

Here, ε_{alloy} is the effective dielectric function of the Au-Ag alloy, $\varepsilon_{Ag}(\lambda)$ and $\varepsilon_{Au}(\lambda)$ are the dielectric function of Ag and Au irradiated at the wavelength λ (355nm) obtained from [10]. ρ_{Ag} is the volume fraction of Ag.

The absorption coefficients of NPs (α) of the four NP substrates (ϕ= 2.5 nm) at 355 nm, was then determined using the calculated effective dielectric functions of the representative NPs with **Eq. S4.1** and **Eq. S4.2**, and the results are summarized in **Table S5**. The calculated absorption coefficients of NPs also correlated well with the experimentally measured normalized UV-

Visible absorbance depicted in **Figure 1(i)**. By plotting the experimentally measured normalized absorbance against the calculated photo absorption coefficient, it was found that they both increased with Ag composition. (**Figure S2)** The calculated photo absorption coefficient agreed well with experimentally measured normalized absorbance.

Table S5. Photo absorption coefficients of AgNPs, Ag55Au45NPs, Ag15Au85NPs, AuNPs

	Real Part of Dielectric Permittivity (ε')	**Imaginary Part of Dielectric Permittivity (ε'')**	**Photo absorption Coefficient at 355 nm (α) (cm^{-1})**
AgNPs	-2.04	0.28	2.98×10^{4}
Ag55Au45NPs	-1.60	3.21	4.86×10^{3}
Ag15Au85NPs	-1.34	4.96	3.62×10^{3}
AuNPs	-1.24	5.60	2.99×10^{3}

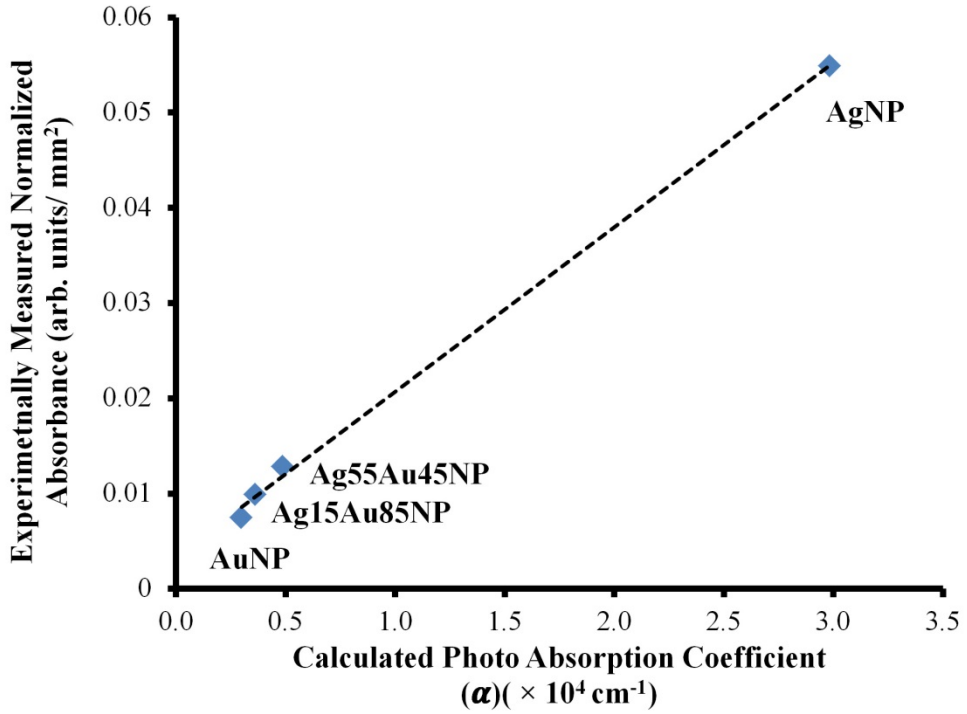

Figure S2. A plot of the experimentally measured normalized absorbance against the computed photo absorption coefficients (at 355 nm) for AuNPs, Ag15Au85NPs, Ag55Au45NPs, and AgNPs

S5. Relationship between Maximum Laser-Induced Heating Temperature of Nanoparticles and Laser Fluence Applied

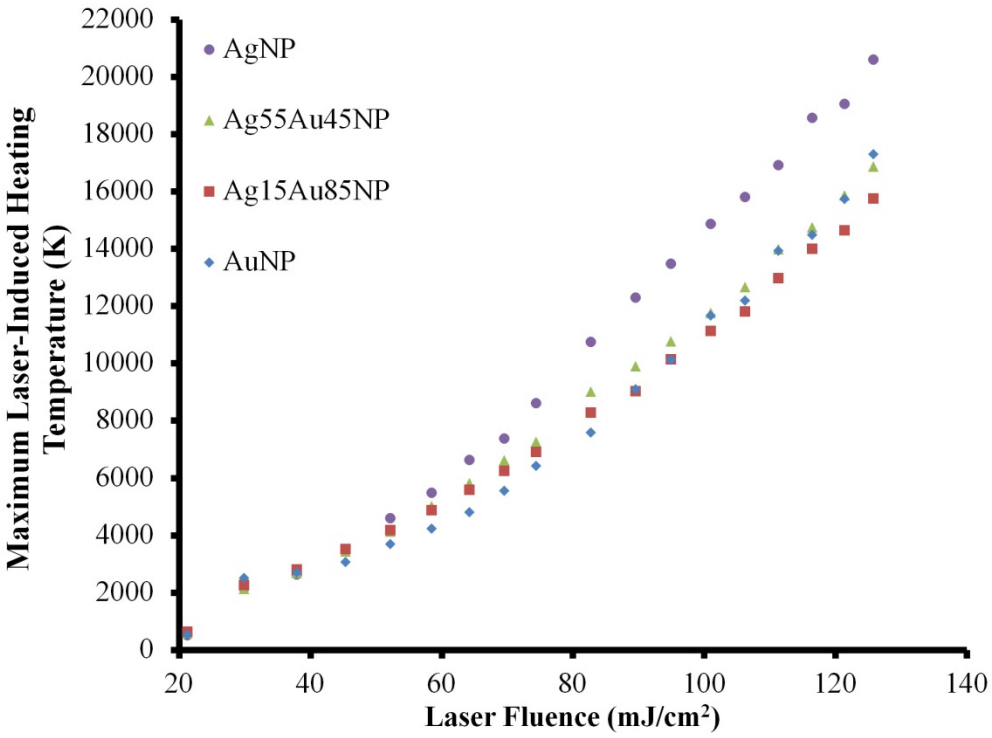

Figure S3. Computed maximum laser-induced heating temperature for AuNPs, Ag15Au85NPs, Ag55Au45NPs, and AgNPs as a function of laser fluence applied (from 21.3 to 125.9 mJ/cm^2).

S6. Determination of Melting Points, Boiling Points and Phase Explosion Temperatures of the Nanoparticles by Molecular Dynamics Simulation

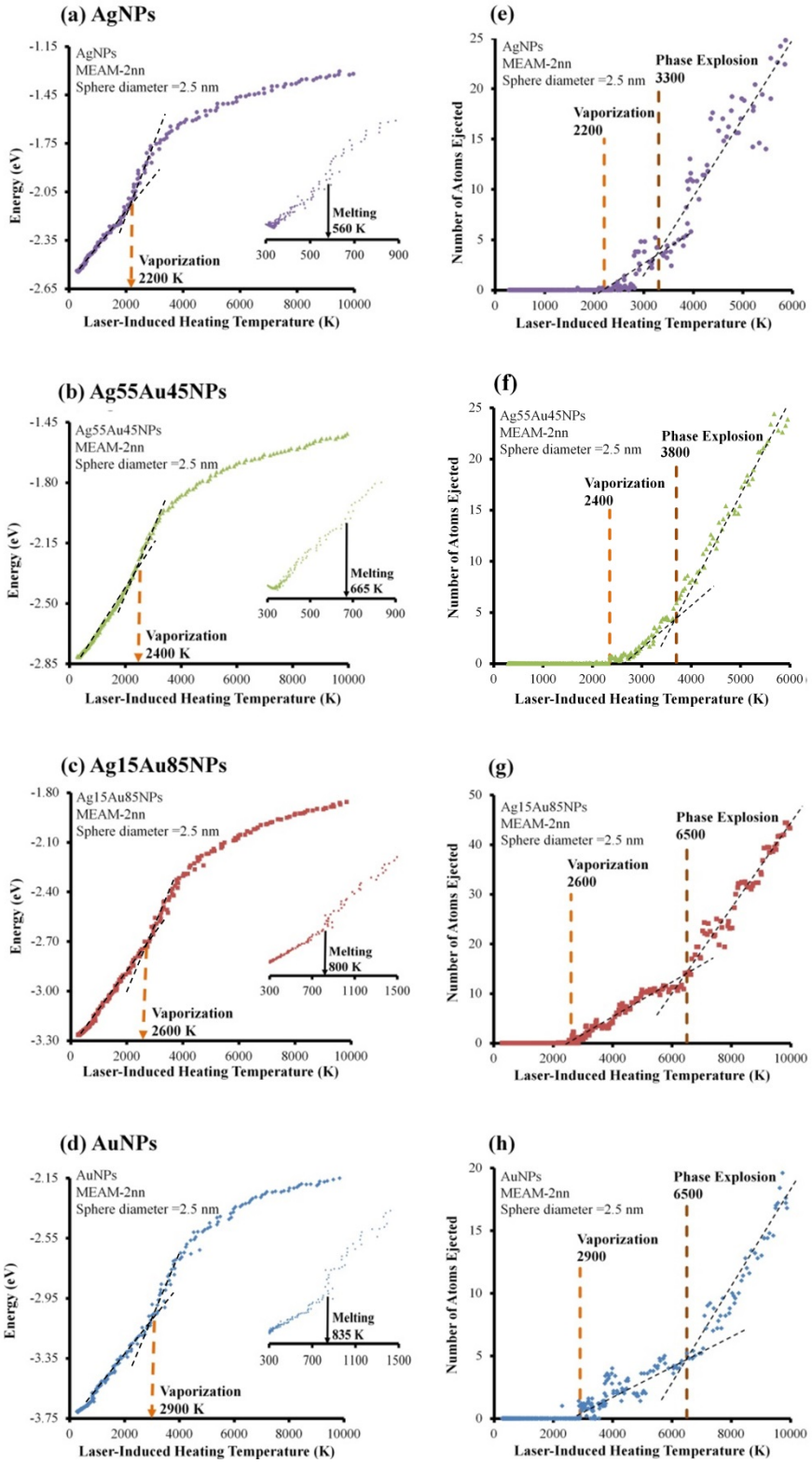

Figure S4. Potential Energies and number of individual metal vapor atoms ablated from AgNPs (a, e) Ag55Au45NPs (b, f), Ag15Au85NPs (c, g), and AuNPs (d, h) as a function of laser-induced heating temperature. The melting points and boiling points could be determined from the sudden change in the slope of the potential energy plot. The phase explosion temperature could be determined from the abrupt increase in atom ejection.

S7. Mass Spectrometric Detection of Metal Ions and Cluster Ions Ablated from Ag-Au Alloy Nanoparticles upon the Laser Irradiation

Table S6. Summary of metal ions and metal cluster ions detected when Ag-Au alloy nanoparticles (i.e. Ag15Au85NPs, Ag55Au45NPs) were irradiated by the pulsed laser.

Metal Ions/ Cluster Ions	**m/z (Relative Abundance)**
Au^+	197 (100%)
Au_2^+	394 (100%)
Au_3^+	591 (100%)
$AuAr^+$	237 (100%)
Ag^+	107 (100%), 109 (91%)
Ag_2^+	214 (50%), 216 (100%), 218 (43%)
Ag_3^+	321 (30%), 323 (100%), 325 (91%), 327 (24%)
Ag_2Cl^+	249 (42%), 251 (100%), 253 (64%), 255 (13%)
$Ag_3Cl_2^+$	391 (16%), 393 (77%), 395 (100%), 397 (54%), 399 (14%), 401 (1%)
$AgAu^+$	304 (100%), 306 (90%)
Ag_2Au^+	411 (52%), 413 (100%), 415 (44%)
$AgAu_2^+$	501 (100%), 503 (94%)

S8. Calculation of Photoabsorption Efficiencies (Q_{abs}) of the Nanoparticles

The photoabsorption efficiencies (Q_{abs}) of AuNPs, Ag15Au85NPs, Ag55Au45NPs, AgNPs can be calculated using their representative dielectric functions. The dielectric functions of the Ag-Au alloys were calculated using a linear relationship on the volume fraction, as expressed in **Eq. S8.1**. [9-10]

$$\varepsilon_{alloy}(\rho_{Ag}, \lambda) = \rho_{Ag}\varepsilon_{Ag}(\lambda) + (1 - \rho_{Ag})\varepsilon_{Au}(\lambda) \qquad \mathbf{Eq.\,S8.1}$$

Here, ε_{alloy} is the effective dielectric function of the Au-Ag alloy, $\varepsilon_{Ag}(\lambda)$ and $\varepsilon_{Au}(\lambda)$ are the dielectric function of Ag and Au irradiated at the wavelength λ. ρ_{Ag} is the volume fraction of Ag.

The photoabsorption efficiency (Q_{abs}) of the four NP substrates at 355 nm, was then determined using the calculated effective dielectric functions of the representative NPs by **Eq. S8.2**, and the results are summarized in **Table S7**. [2, 11]

$$Q_{abs} = q\,\frac{12\varepsilon''}{(\varepsilon'+2)^2+\varepsilon''^2} \qquad \mathbf{Eq.\,S8.2}$$

where $q = R/\lambda$, R is the radius of metal NPs (1.25 nm) and λ is the wavelength of electromagnetic radiation irradiated (355 nm), ε' and ε'' are the real part and imaginary part of the dielectric functions (ε) of pure Au, Ag and Ag-Au alloys.

Table S7. Photoabsorption efficiencies (Q_{abs}) of AgNPs, Ag55Au45NPs, Ag15Au85NPs, AuNPs at the laser irradiation wavelength of 355 nm

	Real Part of Dielectric Permittivity (ε')	Imaginary Part of Dielectric Permittivity (ε'')	Photoabsorption Efficiency (Q_{abs})
AgNPs	-2.04	0.28	0.1479
Ag55Au45NPs	-1.60	3.21	0.0130
Ag15Au85NPs	-1.34	4.96	0.0083
AuNPs	-1.24	5.60	0.0074

References

1 B.-J. Lee; J.-H. Shim; M. Baskes, *Phys. Rev. B,* 2003, **68**, 144112.

2 K.-M. Ng; S.-L. Chau; H.-W. Tang; X.-G. Wei; K.-C. Lau; F. Ye; A. M.-C. Ng, *J. Phys. Chem. C,* 2015, **119**, 23708.

3 P. Buffat; J. P. Borel, *Phys. Rev. A,* 1976, **13**, 2287.

4 S. Little; T. Begou; R. Collins; S. Marsillac, *Appl. Phys. Lett.*, 2012, **100**, 051107.

5 S. Plimpton, *J. Comput. Phys.*, 1995, **117**, 1.

6 M. Baskes, *Phys. Rev. B*, 1992, **46**, 2727.

7 U. Kreibig; M. Vollmer, *Optical Properties of Metal Clusters*; Springer Science & Business Media, **2013**; Vol. 25.

8 J. Bourdon, Growth and Properties of Metal Clusters. Elsevier Scientific: Amsterdam: 1980; Vol. 4.

9 D. Rioux; S. Vallières; S. Besner; P. Muñoz; E. Mazur; M. Meunier, *Adv. Opt. Mater*, 2014, **2**, 176.

10 P. B. Johnson; R.-W. Christy, *Phys. Rev. B*, 1972, **6**, 4370.

11 B. S. Luk'yanchuk; A. E. Miroshnichenko; M. I. Tribelsky; Y. S. Kivshar; A. R. Khokhlov, *New J. Phys*, 2012, **14**, 093022.